5. FLEXURE OF THE LITHOSPHERE

A. ISOSTATIC COMPENSATION

First, we need to go back and look at simple isostatic balances (discussed in Chapter 2, part A) in a slightly different way. Consider the two columns shown in Figure 5.1. The column on the left is a reference column, and the column on the right shows the same crustal section thickened now by a factor of $1/\beta$, where $0 < \beta < 1$. The base of the thickened crust is deflected into the mantle by an amount w due to the weight of the added crust. A local isostatic balance requires that:

$$\rho_m \, g \, w = \left[\frac{1}{\beta} - 1 \right] \rho_c \, g \, t_c \qquad (5.1)$$

where w = vertical deflection of the crust
ρ_m = density of asthenosphere (3300 kg/m^3)
g = gravitational acceleration (9.8 m/s^2)
ρ_c = density of continental crust (2800 kg/m^3)
t_c = thickness of reference crust (35 km)

This result says that the weight of the mountain belt (including the portion that lies below datum) is balanced by a buoyancy force from the mantle. This is a local isostatic balance in that the deflection of the crust at any location depends only on the local amount of crustal thickening at that location. One important shortcoming of the local isostatic balance is that it neglects the lateral strength of the lithosphere. A more realistic (and highly successful) model assumes that the lithosphere responds to loads like an elastic plate overlying an inviscid fluid. The elastic plate corresponds to some poorly defined, colder portion of the thermal lithosphere, whereas the inviscid fluid corresponds to a hotter portion of the lithosphere and the asthenosphere. You should not forget that the elastic plate model is just an extension of the local isostatic compensation model.

B. ELASTIC PLATE FLEXURE

The derivation of the elastic flexure equation is rather involved and, thus, beyond the scope of this course. Those interested can find a detailed but readable derivation in Turcotte and Schubert (1982; their chapter 3). Four basic assumptions are made in deriving the elastic flexure equation. First, the lithosphere is assumed to have a linear elastic rheology. Second, deflections are assumed to be small. Third, the elastic lithosphere is assumed to be thin compared to the horizontal dimensions of the plate. Fourth, planar sections within the plate are assumed to remain planar after deflection. This theory is generally valid for earth's lithosphere. You can, however, run into problems if you apply the theory to certain subduction zones in which large deformations have occurred and stress levels are high. Also, the theory ignores the fact that the viscous asthenosphere has to flow out of the way before the lithosphere can deflect; the theory may not be applicable to areas in which the tectonic load is less than a few million years old.

For the case of a two-dimensional load distribution, such as a linear mountain belt or rift system, the elastic flexure equation reduces to:

$$D \frac{d^4 w}{d x^4} + N \frac{d^2 w}{d x^2} + \rho_m g w = p(x) \qquad (5.2)$$

where x = distance (normal to load axis)
D = flexural rigidity
N = intraplate force (positive if compressive)
p = vertical load distribution

The load distribution will generally vary with distance and includes not only the tectonic loads responsible for the deflection but also the load of water and/or sediment filling the deflection. Closer examination shows that the last two terms in equation 5.2 represent the local isostatic balance given in equation 5.1. The first term, which involves the flexural rigidity, embodies the lateral stiffness of the lithosphere. The larger the flexural rigidity, the smaller the deflection will be under a given load distribution. The second term in equation 5.2 represents the effect of intraplate stress on the deflection. Although this term can be (and usually

is) ignored when modeling lithospheric flexure, it may play an important role in the evolution of stratigraphic sequences at basin margins (see part O of this chapter).

Another way to quantify the rigidity of the lithosphere is to measure its effective elastic thickness, or *EET*. The key word is effective; no one really understands what portion of the lithosphere behaves elastically on a geological time scale. Regardless, the *EET* is related to the flexural rigidity through:

$$EET = \sqrt[3]{\frac{12\,(1-\nu^2)\,D}{E}} \qquad (5.3)$$

where ν = Poisson's ratio (0.25)
E = Young's modulus (7×10^{10} N/m^2)

These two constants (ν and E) characterize the rheology (the stress-strain relationship) of the elastic portion of the crust and mantle lithosphere. For flexural rigidities of 10^{21} N m and 10^{25} N m, the corresponding effective elastic thicknesses are 5.4 km and 117 km, respectively.

The justification for using an elastic plate model is shown in Figure 5.2 (from Watts et al., 1982), where the *EET*, obtained from flexural studies of various tectonic features, is plotted against the age of the load (we will show you how the *EET* is determined at a later point). Points 15, 16, and 17 should be ignored because they are based on averages over continent-size areas and may underestimate the true *EET* for individual features. The *EET* appears to be independent of the age of the load, suggesting that elastic stresses, which cause deflections, do not relax on a geologic time scale. There is, however, evidence that the *EET* depends on the lithosphere's thermal structure. Figure 5.3 (also from Watts et al., 1982) shows that the *EET* is small when the lithosphere is hot and large when the lithosphere is cool. Plots like this one have led many workers (e.g., Caldwell and Turcotte, 1979) to argue that the *EET* is controlled by the depth to a specific isotherm. Although this particular data is for oceanic lithosphere, Watts et al. show that a similar relation to hold for the continents. Again, we want to emphasize that the rocks providing the

lithosphere's long-term strength may not reside entirely in a vertical section of thickness *EET* (e.g., Goetze and Evans, 1979).

C. SIMPLE FLEXURE SOLUTIONS

The most fundamental solutions for equation 5.2 are for a concentrated line load of magnitude V_0 acting on an infinite or semi-infinite (broken) plate (Fig. 5.4). The line load can be thought of as a narrow column of width Δx, height h, and density ρ_L:

$$V_0 = \rho_L g h \Delta x \tag{5.4}$$

The load distribution in equation 5.2 becomes:

$$p(x) = \begin{cases} 0 & x \neq 0 \\ V_0 & x = 0 \end{cases} \tag{5.5}$$

For the case of an infinite plate, the resulting deflection (Turcotte and Schubert, 1982) varies with distance (x) from the load according to:

$$w(x) = \frac{V_0 \alpha^3}{8D} \exp\left(-\frac{x}{\alpha}\right)\left[\cos\left(\frac{x}{\alpha}\right) + \sin\left(\frac{x}{\alpha}\right)\right] \tag{5.6}$$

for nonnegative values of x. As you might expect, the deflection is symmetric about $x = 0$ (Fig. 5.4A). The quantity α is known as the flexural parameter and has units of length. The flexural parameter is related to the flexural rigidity through the relationship:

$$\alpha = \sqrt[4]{\frac{4D}{\rho_m g}} \tag{5.7}$$

and plays an important role in controlling the deflection's width. This is due to the exponential term in equation 5.6. When the distance α is small, the deflection is narrow; when α is large the deflection is broad. Figure 5.4A shows that the half-width of the deflection (defined as the distance from the point load to the first datum-crossing) is $3\pi\alpha/4$. At $x = 0$, the magnitude of the deflection is $w_0 = V_0\alpha^3/8D$. The maximum deflection is

deeper when the plate is weaker. This solution is valid only when the width of the load (Δx) is small compared to α. We will look at some solutions for distributed loads later on. A forebulge of low amplitude that lies adjacent to the depression (at a distance of $\pi\alpha$ from the load) is due to the interplay between the lithosphere's rigidity and the mantle buoyancy force.

Figure 5.4B shows the solution to the elastic flexure equation (equation 5.6) for the case when the lithosphere is broken at the point where the line load is applied ($x = 0$). What we mean by broken is that no stress is transferred across the break. In this situation, the weight of the line load is shared equally by the two semi-infinite plates. The deflection (Turcotte and Schubert, 1982) is described by:

$$w(x) = \frac{V_0 \alpha^3}{4D} \exp\left(-\frac{x}{\alpha}\right) \cos\left(\frac{x}{\alpha}\right) \tag{5.8}$$

where α is given by equation 5.7. Notice that the maximum deflection of the broken plate is $V_0\alpha^3/4D$, twice that of the infinite plate. Also, the half-width of a deflection on a broken plate ($\pi\alpha/2$) is narrower than on a continuous plate.

D. FOREBULGES

Forebulges receive a great deal of attention. They have many names, including outer bulge and peripheral bulge. Forebulges were first recognized seaward of oceanic trenches and near volcanic islands and aseismic ridges. Forebulges seem to be more difficult to observe on the continents, perhaps due to erosion and preexisting topography. Certain basement arches, located between two or more basins, may be due to the constructive interference of forebulges associated with the individual basins (Quinlan and Beaumont, 1984). Figure 5.5 shows an elastic deflection caused by two parallel line loads acting on an infinite plate. The line loads are separated by a distance of $2\pi\alpha$, so the forebulges lying between the loads constructively interfere. The amplitude of the central forebulge is twice the amplitude of the peripheral forebulges. Armin (1987) suggests that a forebulge is the source for Lower Permian conglomerates in the Pedregosa foreland basin of northern Mexico and the

southwestern United States. Many unconformities in foreland basins have been attributed to uplift on forebulges (Jacobi, 1981; Quinlan and Beaumont, 1984; and Tankard, 1986).

Figure 5.6 (from Peterman and Sims, 1988) shows the Goodman swell in northern Wisconsin. The Goodman swell is defined by an biotite age anomaly in crystalline rocks. Rocks on the swell are some 700 My younger than rocks in surrounding areas but similar in age to mafic rocks in the Midcontinent rift (1090 to 1120 Ma). Peterman and Sims suggest that the Goodman swell represents a forebulge amplified through constructive interference. Their argument is compelling; the swell is in a perfect location for constructive interference between three segments of the midcontinent rift (rift axis is marked by a heavy dashed line in Fig. 5.6). Uplift and erosion at the swell would have carried rocks through the biotite blocking temperature, thereby explaining the young ages on the swell that coincide with the age of the rift. It would be interesting to calculate the amount of differential erosion required to create the age anomaly.

E. SEDIMENT AND WATER LOADS

Although we have created deflections using a line load, we have not yet made any allowance for the weight of the sediment or water that fills the deflection (effectively, we have thus far assumed the deflections to be filled by air). If sediment of density ρ_s fills the deflection to the original datum, then the load distribution can be expressed (approximately) as:

$$p(x) = \rho_s g w(x) + \begin{cases} V_0 & x = 0 \\ 0 & x \neq 0 \end{cases} \tag{5.9}$$

The weight of the sedimentary section can be transferred to the left-hand side of equation 5.2 and incorporated into the buoyancy term. The solution of this new equation will have the same form as equation 5.4 or 5.8 with the exception that the flexural parameter is defined differently:

$$\alpha = \sqrt[4]{\frac{4D}{(\rho_m - \rho_s)g}} \qquad (5.10)$$

Adding a sediment or water load to the deflection causes α to increase, thereby increasing the deflection's magnitude and width. None of this is surprising. Increasing the load on the lithosphere will always make the deflection deeper, and adding loads far from the central line load should surely increase the width of the deflection. This technique for incorporating sediment and water loads is somewhat suspect in that equation 5.9 assumes that sediment is removed from the forebulges (where $w < 0$). Typical values for the flexural parameter (in km) are:

	Air	Water	Sediment ρ_s = 2500 kg/m^3
D = 10^{21} N m	18.7	20.5	26.7
D = 10^{25} N m	187.	205.	267.

It is interesting to note that deflections are very narrow for flexural rigidities of 10^{21} N m and smaller. Although the magnitude of the rigidity is a large number, the load is almost locally compensated.

F. EXAMPLE I--A FICTITIOUS AULOCOGEN

Consider the section of rifted crust shown in Figure 5.7. Rifting has replaced a portion of the crust with mantle rock. This means that the rift is not in isostatic equilibrium with the adjacent unrifted crust. If we assume that no (locally compensated) initial subsidence took place, the entire excess weight of the rift zone must be compensated regionally by lithospheric flexure. The point of this exercise is to figure out an average value for β given the geometry of the flexural basin overlying the rift. Both the idea and the basin dimensions for this example come from a comprehensive study of gravity and flexure in the middle Amazon Basin, Brazil, by Nunn and Aires (1988).

Following equation 5.4, the magnitude of the tectonic load can be expressed as the density contrast between mantle and crust multiplied by the gravitational acceleration and cross-sectional area of the intrusion:

$$V_0 = (\rho_m - \rho_c)\, g\, r\, t\, (1 - \frac{1}{\beta}) \tag{5.11}$$

We are making a leap of faith by approximating the excess load of a broad rift as a concentrated line load. We will address that problem later on. Some additional assumptions are:

- Deflection is filled to datum with sediment (ρ_s = 2500 kg/m^3)
- Half-width of basin = 225 km
- Maximum depth = 6 km
- Normal crustal thickness = 50 km
- Width of rift zone = 150 km

Using the half-width we can solve for the flexural parameter:

$$\alpha = \frac{4\,(225\ km)}{3\,\pi} = 95.5\ km \tag{5.12}$$

then the flexural rigidity

$$D = \frac{1}{4}\,\alpha^4\,(\rho_m - \rho_s)\,g = 1.6 \times 10^{23}\ N\text{-}m \tag{5.13}$$

and the effective elastic thickness

$$EET = \left[\frac{12\,D\,(1 - \nu^2)}{E}\right]^{1/3} = 29.7\ km \tag{5.14}$$

Knowing the maximum depth, D, and α we can now calculate V_0:

$$V_0 = \frac{8\,D\,(6000\ m)}{\alpha^3} = 8.8 \times 10^{12}\ \frac{N}{m} \tag{5.15}$$

and the stretching factor

$$\beta = \left[1 - \frac{V_0}{(\rho_m - \rho_c)\, g\, r\, t} \right]^{-1} = 1.3 \qquad (5.16)$$

For comparison, if the rift was isostatically compensated (in a local sense, with $D = 0$) the basin would be only 150 km wide (i.e., the width of the rift) and have an average depth of:

$$w = \frac{(\rho_m - \rho_c)}{(\rho_m - \rho_s)}\, t \left(1 - \frac{1}{\beta}\right) = 7.2 \ km \qquad (5.17)$$

rather than a maximum depth of 6 km. We will return to this example after discussing how to calculate deflections under distributed loads. Nunn and Aires (1988) found that the middle Amazon Basin's *EET* is in the range from 20 to 25 km.

G. DISTRIBUTED LOAD DISTRIBUTIONS

There are relatively few geologic situations to which the point-load solution can be directly applied. Typically, loads are distributed over a broad area (e.g., mountain belts) rather than concentrated. However, as long as the lithosphere can be treated as an infinite plate, complicated load distributions can broken into a large number of line loads, and the deflection can be calculated by adding up the deflections caused by each line load. This method is based on the linearity of equation 5.2 and is sometimes referred to as a convolution.

Consider the load distribution $p(x)$ shown in Figure 5.8. If this distribution is represented by a set of line loads with spacing Δx, then the line load at some position x will be $V_x = p(x)\ \Delta x$. In analogy to equation 5.6, the incremental deflection, measured at x_0, that results from this point load will be:

$$\Delta w_1(x_0) = \frac{p(x)\, \alpha^3\, \Delta x}{8D}\, exp\left(-\frac{x_0 - x}{\alpha}\right)\left[cos\left(\frac{x_0 - x}{\alpha}\right) + sin\left(\frac{x_0 - x}{\alpha}\right)\right] \qquad (5.18a)$$

when $x < x_0$ and

$$\Delta w_2(x_0) = \frac{p(x)\,\alpha^3\,\Delta x}{8D}\,exp\left(-\frac{x-x_0}{\alpha}\right)\left[\cos\left(\frac{x-x_0}{\alpha}\right) + \sin\left(\frac{x-x_0}{\alpha}\right)\right] \qquad (5.18b)$$

when $x > x_0$. Two versions are required because the original solution (equation 5.6) assumed a positive argument in the exponential. The total deflection is obtained by summing up the appropriate incremental deflections. In the limit of an infinitely small Δx, the summation becomes an integration:

$$w(x) = \int_{-\infty}^{x} d\,w_1(x) + \int_{x}^{\infty} d\,w_2(x) \qquad (5.19)$$

In principle the limits of integration go from -∞ to +∞; in practice, the limits are determined by the width of the load distribution. Equation 5.19 assumes that the plate is continuous, not broken. To model a broken plate, some extra terms must be added to equation 5.18, to ensure that no net bending moment or shear force exists at the break. The interested reader can refer to Hetenyi (1946) for more details.

H. RECTANGULAR LOAD DISTRIBUTION

A simple, but useful, load distribution to consider is a rectangular distribution (Fig. 5.9):

$$p(x) = \begin{cases} p_0 & |x| \le L \\ 0 & |x| > L \end{cases} \qquad (5.20)$$

This one is easy to deal with because $p(x)$ is constant between $x = -L$ and $x = +L$ and 0 elsewhere. Assuming that $p(x)$ represents a layer of thickness h_L and density ρ_L and that the deflection is filled with sediment then the deflection is given by:

$$w(x) = \frac{\rho_L\,h_L}{2(\rho_m - \rho_s)}\left[2 - exp\left(-\frac{x+L}{\alpha}\right)\cos\left(\frac{x+L}{\alpha}\right) - exp\left(-\frac{L-x}{\alpha}\right)\cos\left(\frac{L-x}{\alpha}\right)\right] \qquad (5.21)$$

for $0 < x < L$ and

$$w(x) = \frac{\rho_L h_L}{2(\rho_m - \rho_s)}\left[exp(-\frac{x-L}{\alpha}) cos(\frac{x-L}{\alpha}) - exp(-\frac{x+L}{\alpha}) cos(\frac{x+L}{\alpha})\right] \quad (5.22)$$

for $x > L$. Once again, the deflection is symmetric about $x = 0$. Using equation 5.21, you can show that the deflection at $x = 0$ is:

$$w(0) = \frac{\rho_L h_L}{(\rho_m - \rho_s)}\left[1 - exp(-\frac{L}{\alpha}) cos(\frac{L}{\alpha})\right] \quad (5.23)$$

When L is large compared to α equation 5.23 reduces to:

$$w(0) = \frac{\rho_L h_L}{(\rho_m - \rho_s)} \quad (5.24)$$

This result suggests that, near its center, the load is locally compensated when the load is very broad and/or the flexural rigidity is negligibly small. This behavior occurs because every bit of the plate is loaded equally near the middle of the rectangular load distribution. There is simply no unencumbered part of the plate near enough to help support the load. Under the center of the load distribution, a deflection close to that predicted by a local isostatic balance can be attained, even though D is not small. Evaluation of equation 5.23 shows that local compensation occurs (approximately) at $x = 0$, when $L > 1.5\ \alpha$. The situation is quite different near the edge of the load ($x = L$). Here, the deflection is given by:

$$w(L) = \frac{\rho_L h_L}{2(\rho_m - \rho_s)}\left[1 - exp(-\frac{2L}{\alpha}) cos(\frac{2L}{\alpha})\right] \quad (5.25)$$

Even if L is large compared to α, the deflection is only one-half of that expected for a locally compensated load. Equation 5.25 shows that, no matter what the width, the entire load distribution can never be locally compensated. Note that if L is very small compared to α, the deflections in both equations 5.23 and 5.25 reduce to zero (assuming everything else is held constant). Narrow loads are supported by the strength of the lithosphere, whereas broad loads are supported by the mantle's buoyancy.

One last consideration is the relation of the flexural parameter to the half-width of the basin (call it x_0) that is created by the rectangular load distribution. As before, x_0 will be the location where the deflection first crosses the datum: $w(x_0) = 0$. Using equation 5.22, we see that this requires:

$$exp(-\frac{x_0 - L}{\alpha}) \cos(\frac{x_0 - L}{\alpha}) = exp(-\frac{x_0 + L}{\alpha}) \cos(\frac{x_0 + L}{\alpha}) \qquad (5.26)$$

Don't bother trying to solve directly for α; it can't be done. This is another example of a transcendental equation. The best you can do is to isolate one α and then iterate to obtain a solution:

$$\alpha = \frac{x_0 - L}{\cos^{-1}\left[exp(-\frac{2L}{\alpha}) \cos(\frac{x_0 + L}{\alpha}) \right]} \qquad (5.27)$$

We will show you how to solve for α in the following example.

I. EXAMPLE II--THE AULOCOGEN RECONSIDERED

With the solutions from the last section in hand, we are ready to go back and look again at the estimates for flexural rigidity (1.6×10^{23} N m) and the crustal stretching factor (1.3) that we obtained in part G of this chapter. In that section we approximated the load of a mantle intrusion, under the aulocogen as a concentrated line load:

- Deflection is filled to datum with sediment (ρ_s = 2500 kg/m^3)
- Half-width of basin = 225 km
- Maximum depth = 6 km
- Normal crustal thickness = 50 km
- Width of rift zone = 150 km

The first step is to determine α given the information that L = 75 km and x_0 = 225 km. Make an initial guess of α = 10 km, and substitute these values into the right-hand side of equation 5.27 to obtain a new value for α. If this new value equals 10 km then you are done. You made a lucky guess. If the new value is not 10 km, substitute the new value back into

the right-hand side of equation 5.27. Repeat this process until α stops changing. Our sequence goes: 10.0, 95.5, 84.3, 86.1, 86.4, 86.3, 86.3; the sequence converges to:

$$\alpha = 86.3 \ km \tag{5.28}$$

which is not radically different from our previous estimate of 95.5 km. The flexural rigidity and effective elastic thickness are:

$$D = 1.1 \ x \ 10^{23} \ N \ m \tag{5.29}$$

and

$$EET = 26.0 \ km \tag{5.30}$$

You can see that we were well justified in using the point load model in Example I to estimate the flexural rigidity. Letting $\rho_L = \rho_m - \rho_c = 500$ kg/m^3, we can now use equation 5.23 to determine the amplitude of the tectonic load (h_L):

$$h_L = \frac{(\rho_m - \rho_s)(6.0 \ km)}{(\rho_m - \rho_c)\left[1 - exp(-\frac{L}{\alpha}) \ cos(\frac{L}{\alpha})\right]} = 13.2 \ km \tag{5.31}$$

and, from the rift's geometry (Fig. 5.7), the stretching factor

$$\beta = \frac{t}{t - h_L} = 1.4 \tag{5.32}$$

This β is somewhat larger than the value of 1.3 that we obtained using the line-load model. The difference shows that a smaller concentrated load is required to explain the same maximum deflection obtained using a distributed load. Deflections for the line and rectangular loads are shown in Figure 5.10. The deflections are nearly identical. Our earlier representation of the rift zone by a line load is entirely adequate. The simpler model of the basin works even though the load distribution's half-width (75 km) is comparable in size to the flexural parameter (86 km). When building models, remember the words of Martin Luther: "Sin

boldly and frustrate the Devil; protected by your faith, he or she cannot touch you." A simple back-of-the-envelope calculation sometimes can be as revealing as a more sophisticated model that requires a computer.

J. EXAMPLE III--FLEXURAL UPLIFT DUE TO EROSION

Figure 5.11 (from Hamblin and Rigby, 1969) shows a cross section perpendicular to the Grand Canyon of the Colorado River. We want to calculate how much flexural uplift has occurred at the canyon margins due to sediment removal by the Colorado River. To a casual modeler, the canyon is a two-dimensional ditch of rectangular cross section. Assume that the canyon has an average width of 9 km, an average depth of 0.5 km, and that the eroded sediment had a density of 2500 kg/m^3. Because we don't know what flexural rigidity is appropriate for this region, we will do the calculation for both $D = 10^{21}$ and 10^{25} N m.

The appropriate deflection equation is 5.25, which gives the deflection, of an infinite plate, at the edge of the rectangular load distribution. The amplitude and density of the load are -500 m and 2500 kg/m^3, respectively. The half-width is 4500 m. This should all be clear; the load is the sediment removed by the river. What is the appropriate choice for α? You might be tempted to use equation 5.10, which contains the density contrast between mantle and sediment. Don't. We have already put the eroded sediment into the load. The only material on the surface being displaced by the flexure is air, which has a negligible density. Get α from equation 5.7. The resulting deflections are

$$w(L) = -85.6\ m,\ for\ D = 10^{21}\ N\ m \tag{5.33}$$

and

$$w(L) = -18.2\ m,\ for\ D = 10^{25}\ N\ m \tag{5.34}$$

Negative deflections indicate uplift. These numbers represent flexural uplift of the entire lithosphere and do not include contributions from elastic relaxation of rocks in the canyon walls. We have not checked to see whether or not flexural uplift can be recognized on topographic profiles across the canyon.

K. EXAMPLE IV–THRUST BELTS AND FORELAND BASINS, THE APENNINES

Figure 5.12A (from Royden and Karner, 1984) shows a cross section through the Apennine mountains and the adjacent foreland sedimentary basin. The curved line on the right-hand-side of the figure represents the base of the Pliocene sedimentary sequence as determined from drilling and seismic reflection profiles. Royden and Karner argue that the underlying Miocene sediments were deposited near sea level and are now flexed downward due to emplacement of the adjacent thrust belt. Our first task is to determine whether or not the thrust belt is sufficiently heavy to explain the observed deflection.

The best way to start is to approximate the topographic load of the thrust belt by a rectangular load. You may find this approximation unpalatable, but it's actually pretty accurate. From Figure 5.12A, reasonable parameters are L = 55 km and h_L = 1.5 km. If you smooth the basal Pliocene surface and extend it to sea level, the width of the deflection appears to be about x_0 = 150 km. Assume that the deflection is filled with sediment with a density of 2500. kg/m^3. With this information, we can calculate α using equation 5.27. The sequence goes 10.0, 60.5, 55.0, 56.4, 56.0 56.1, and 56.1 so that:

$$\alpha = 56.1 \ km \tag{5.35}$$

$$D = 1.9 \, x \, 10^{22} \ N\text{-}m \tag{5.36}$$

$$EET = 14.6 \ km \tag{5.37}$$

An implicit assumption in this calculation of α is that no sediment is deposited above datum. Some foreland basins may be overfilled, in which case this assumption will not be valid. Near the thrust belt's edge the basal Pliocene surface lies at a depth of over 8 km. Using equation 5.25 and the flexural parameter determined above, we predict a deflection of only:

$$w(L) = 2.5 \ km \tag{5.38}$$

This calculation shows that the load of the thrust belt and basin sediments is insufficient (by a factor of three, at least) to explain the observed deflection in the foreland. Royden and Karner (1984) tried to increase the calculated deflection in a number of ways (including, breaking the plate under the mountains and varying the density of the sediment) but, to no avail. The topographic load is just too small. Royden and Karner finally fitted the deflection by applying a concentrated line load under the mountains (Fig. 5.12B). They hypothesized that this load represents the weight of a subducted slab attached to the Apennine foreland lithosphere. Figure 5.13 shows the predicted deflection of the basal Pliocene surface as calculated from equations 5.21 and 5.22. A maximum deflection of less than 4 km is attained under the mountains.

Figure 5.14 shows an alternative view of foreland basin development (in a forearc setting) from Stockmal et al. (1986). Royden and Karner (1984) assume that the thrust belt is constructed on a horizontal surface, whereas Stockmal et al. (1986) argue that a preexisting ocean basin must be filled in also. Replacement of water with sediment and crustal slivers loads the lithosphere. Let's see if this new load (which is really an integral part of the thrust belt) can give us the additional deflection we need in the Apennine foreland basin. If we assume that the edge of the former ocean basin coincides with the edge of the thrust belt, we can determine the deflection using equation 5.25 again. The edge of the ocean basin was probably farther west (shallow water Miocene sediments are exposed in the thrust belt), but this assumption simplifies our calculations. Assume also that the width of the ocean basin was very large compared to the flexural parameter ($2L >> \alpha$) and that the ocean basin had a depth of 5 km. The amplitude of the load is then h_L = 5 km and the deflection is given by:

$$w(L) = \frac{\rho_L h_L}{2(\rho_m - \rho_s)} \tag{5.39}$$

Because the ocean basin was presumably in isostatic equilibrium, the appropriate load density is $\rho_L = \rho_s - \rho_w$. The load arises because sediment replaces water in the basin. We are also assuming that sediment fills the deflection caused by this new load. The resulting deflection is:

$$w(L) = 4.7 \ km \tag{5.40}$$

Figure 5.15 shows the predicted deflection. Adding the deflection from equation 5.40 to the deflection associated with topography (from equation 5.38) gives a total deflection of:

$$w_T(L) = 4.7 + 2.5 = 7.2 \ km \tag{5.41}$$

which is much closer to our estimate of 8 to 10 km from Figure 5.12. Filling the ocean basin with rock of crustal density (2800 kg/m^3) will increase the deflection that we calculated in equation 5.40. Deep seismic surveys may help to discriminate between the two models for the Apennines, but you can be reasonably sure that the truth lies between these extremes. You should not apply the Stockmal et al. (1986) model to all foreland basins. Retroarc forelands such as the Andean and Cretaceous western interior basins were never adjacent to an ocean basin. Indeed, Lyon-Caen et al. (1985) show that the topographic load of the sub-Andes mountains is sufficient to cause the lithospheric deflection that is inferred from gravity anomalies over the Andean foreland basin.

Consider the fate of the foreland basin as the Apennine mountains are eroded away. As the topographic load diminishes, the basin will rebound, causing sediment to be eroded from the basin. Even after the mountains are gone, however, a 4- to 5-km-deep foreland basin will remain.

L. AN ALGORITHM FOR COMPUTING DEFLECTIONS

The previous examples show that you can get a lot of mileage out of simple solutions to the elastic flexure equation. Nevertheless, there will be situations in which the load distribution is not adequately represented by a simple rectangle. For these cases we present you with a general algorithm for solving the flexure equation. This algorithm is not very sophisticated, but it is based on solutions for a rectangular load that we have already developed. Also, this algorithm has been used in the literature (e.g., Jordan, 1981) to model sedimentary basins. For most of our work, we prefer to calculate deflections using finite-difference approximations to the elastic flexure equation. Finite-difference algorithms can be written in a very general manner, allowing us to model

broken plates, lateral variations in the basin-fill density and the flexural rigidity, and intraplate stress fluctuations.

Begin by choosing N points on the elastic plate with a uniform spacing of Δx. A rectangular load of width Δx will be placed at each point, and deflections will be calculated at these points. The spacing Δx should be small compared to the flexural parameter (α) and small enough to adequately characterize the primary load distribution. The points should be evenly distributed about the load and extend to a distance of roughly 3α on either side of the load. An adequate compromise between resolution and computing time is N = 100 and Δx = 10 km.

Figure 5.16 is a schematic showing how the loads are represented. At any point j the load will be determined by specifying either the thickness of the load h_j or the topography t_j (where $t_j = h_j - w_j$) and the density of the load ρ_j. The load at point j will cause a deflection at point k of w_{kj}. Calculating the total deflection at point k involves doing the sum:

$$w_k = \sum_{j=1}^{N} w_{k\,j} \tag{5.42}$$

The incremental deflection w_{kj} is calculated from:

$$w_{k\,j} = \rho_j h_j G_{k-j} \tag{5.43}$$

where G_{k-j} has two forms

$$G_{k-j} = \left[1 - exp(-\frac{\Delta x}{2\alpha}) \cos(\frac{\Delta x}{2\alpha}) \right] \Big/ \rho_m \tag{5.44}$$

if k equals j and

$$G_{k-j} = \left\{ exp\left[-(|k-j|-\frac{1}{2})\frac{\Delta x}{\alpha}\right] \cos\left[(|k-j|-\frac{1}{2})\frac{\Delta x}{\alpha}\right] \right.$$

$$\left. - exp\left[-(|k-j|+\frac{1}{2})\frac{\Delta x}{\alpha}\right] \cos\left[(|k-j|+\frac{1}{2})\frac{\Delta x}{\alpha}\right] \right\} \Big/ 2\,\rho_m \tag{5.45}$$

if k does not equal j. The computational process can be speeded up considerably if you realize that there are only N distinct values of G to be calculated (because $G_{k-j} = G_{j-k}$). These are $G_0, G_1, G_2, \ldots, G_{N-3}, G_{N-2}, G_{N-1}$. Having calculated them once, just store their values someplace and look them up as needed when calculating deflections. Equation 5.44 is just the equation for the deflection under the center of a rectangular load of unit height and density and width Δx (equation 5.23). Equation 5.45 is derived from equation 5.22, which gives deflections for points located beyond the rectangular load. The appropriate form of α is given by equation 5.7; the weight of the basin fill is included in the h_j terms.

Probably the best way to illustrate the algorithm is to consider the specific example of a thrust belt shown in Figure 5.17. The primary load is a rectangular thrust plate with a thickness of 3 km and density of 2500 kg/m^3. The length of the thrust plate is 110 km, and the rigidity of the lithosphere is $D = 10^{23}$ N m. We use $N = 101$ and $\Delta x = 10$ km. The thrust plate load is located at points 45 through 55. Sediment of density 2300 kg/m^3 fills the deflection to the original datum. In making these assumptions, we are setting the following conditions:

$$t_i = 0 \tag{5.46}$$

and

$$\rho_i = 2300\ kg/m^3 \tag{5.47}$$

for i = 1, 2, ..., 44 and 56, 57, ..., 101 and:

$$h_i = 3\ km \tag{5.48}$$

and

$$\rho_i = 2500\ kg/m^3 \tag{5.49}$$

for i = 45, 46, ..., 55.

First, calculate the deflection using only the primary load, the thrust plate. The resulting deflection is shown in Figure 5.18A. What thickness

of sediment (Δh_i) is needed to fill the deflection? This is calculated using:

$$\Delta h_i = (t_i + w_i) - h_i \tag{5.50}$$

for i = 1, 2, ..., 44 and 56, 57, ..., 101. If Δh_i is positive, add this amount to the existing load at the appropriate points and calculate the resulting deflection. Repeat this last step of filling in the deflection and then recalculating the deflection, until the deflection stops changing. Figure 5.18B shows the deflection after 20 iterations. Note that this scheme fills the deflection, but does not erode the forebulges. This is a fairly general algorithm. By setting the t_i to some nonzero value initially, you can build a topographic slope over the basins. You can also specify that the primary load be built up to some given level of topography simply by filling in or removing material over the primary load.

M. EXAMPLE V--FLEXURAL BACKSTRIPPING

In Chapter 3, part E, we calculated a quantity called tectonic subsidence based on the assumption that the sedimentary column was in local isostatic compensation throughout its evolution. From what we've seen so far, local compensation is approximated only in young hot rift basins where the rigidity is low and faults are active, and in basins where sedimentary strata vary little in thickness over distances large compared to the flexural parameter. In Figure 5.19, we show the tectonic subsidence associated the thrust belt and foreland basin discussed in the previous section. The primary load is a 3-km-thick by 110-km-wide thrust plate with a density of 2500 kg/m^3. In keeping with our previous definition of tectonic subsidence, the deflection is filled with water. For comparison we also show the tectonic subsidence predicted for the case of Airy compensation. The Airy backstripping curve was obtained by dividing the total subsidence by 2.3, the ratio of the density differences, as discussed in Chapter 2. Near the basin axis, tectonic subsidence calculated using the Airy compensation assumption is considerably less than the true tectonic subsidence, whereas in the distal part of the basin the Airy curve predicts tectonic subsidence where none has occurred.

Many workers have presented graphs purporting to show tectonic subsidence, using the Airy compensation model, for foreland basins (we even show some in these notes). When evaluating these graphs, you should keep in mind that foreland basins are present largely because the adjacent mountain belt is flexurally compensated. A particularly obnoxious problem is that these plots may cause you to overestimate the ages of fault displacement simply because the Airy backstripping scheme predicts tectonic subsidence where none has yet occurred.

In Chapters 3 and 4, we calculated tectonic subsidence in rift basins using the assumption of Airy isostasy. If the *EET* of rifted lithosphere increases as thermal relaxation progresses (see Fig. 5.3), then the weight of the rifted crust will be spread over a progressively wider area. If this process actually occurs, then Airy backstripping schemes will tend to underestimate tectonic subsidence within the rift basin and overestimate tectonic subsidence adjacent to the rift basin. Flexural backstripping is a murky process because the rheology of the continental lithosphere is not well understood. In the next section, we will discuss how the stratigraphy of passive margins might be influenced by secular variation in the lithosphere's rigidity.

N. PASSIVE MARGIN STRATIGRAPHY

Figure 5.20 (from Watts and Thorne, 1984) shows that middle to late Mesozoic sediments on the east coast of the United States onlap progressively onto the continent. One interpretation of this data is that the width of the deflection increased as the lithosphere cooled and thickened following rifting. To a rough approximation, the data in Figure 5.3 suggests that the *EET* (expressed in km) increases with time since rifting (expressed in My) as:

$$EET = 3.\sqrt{t} \tag{5.51}$$

Over the first 100 My of cooling the lithosphere's *EET* will increase from zero to thirty kilometers. The corresponding increase in the flexural rigidity (from equation 5.3) is from 0 to 1.7×10^{23} N m. We assume that the distance between the point of onlap and the edge of the rift is given by:

$$\Delta X = \frac{3\pi}{4}\alpha \qquad (5.52)$$

Remember, this is the half-width of the deflection caused by a line load on an infinite elastic plate. If we assume that the basin is filled with sediment of density 2500 kg/m^3, ΔX increases from 0 to 227 km. This calculation assumes that the basin is not overfilled, which may not be true for Late Cretaceous strata. The calculation does not explain the seaward shift in onlap observed for Cenozoic sediments. It is, however, interesting to note that much of the observed onlap may be associated with cooling of the lithosphere following rifting.

As you might expect, there are other ways to explain the onlap in Figure 5.20. The most obvious is a long-period transgression followed by a regression.

O. INTRAPLATE STRESS

Intraplate stress is a manifestation of the tectonic forces that cause plates to move over the surface of the earth. Until recently, the effect of these stresses on the evolution of sedimentary basins has been ignored. Most workers will agree that intraplate stress plays a primary role in the formation of thrust belts and rifts, but the stress itself has been thought to play only an insignificant role in the vertical deflection of the lithosphere. However, recent work by Cloetingh et al. (1985), Cloetingh (1986), and Karner (1986) shows that variations in intraplate stress level may have an substantial influence on the stratigraphic evolution of sedimentary basins. The effect of a compressional intraplate stress on flexed lithosphere is easy to envision. Hold a ruler flexed slightly between your hands. Move your hands together by a small amount and observe what happens. The deflection is amplified. In effect, a compressional stress reduces the plate's rigidity whereas a tensional stress increases the plate's rigidity.

Figure 5.21 (from Cloetingh et al., 1985) shows the effect of intraplate stress variations on a hypothetical passive margin. The margin subsides through time because of thermal contraction and sediment loading. The flexural rigidity of the margin is assumed to increase from

zero as the margin cools so that, at 30 my after rifting, EET = 22 km. When a tensional stress is applied to the margin, uplift occurs within the basin and subsidence on the basin flanks; intraplate stress variations have an opposite effect on the basin's axis and flanks. As the plate continues to cool and stiffen, intraplate stress will have a diminished capacity to cause deflections. It is important to emphasize that low levels of intraplate stress can cause deflections only when the plate has already been deflected by vertically applied loads.

Braun and Beaumont (1989) construct a rift basin model wherein the lithosphere's strength varies with depth, and the lithosphere's rigidity is finite, even during extension. In this model, the rift basin can be initially over- or undercompensated, depending on the depth at which the lithosphere's strength is concentrated. Their model differs from McKenzie's simple stretching model which assumes the rift basin is isostatically compensated during extension. In the Braun and Beaumont model, the effect of intraplate tension on the basin is to cause uplift if the rift is overcompensated, and subsidence if the rift is undercompensated. The lesson here is, if you want to really understand how a specific intraplate stress variation affects basin stratigraphy, you need to know a number of things (deformation mechanism, temperature, lithology, pore pressure, among others) that influence the lithosphere's rigidity. You can read Cloetingh (1988) to learn more about this problem.

We are convinced that intraplate stresses can and do play an important role in determining basin stratigraphy. One recurring theme in the geologic literature for the United States Rocky Mountains is the widespread, but subtle, reactivation of older, commonly Precambrian, structures throughout Phanerozoic time. A detailed paleocurrent study of the Morrison Formation, for example, led Peterson (1984) to suggest that subtle uplifts and depressions were developing in central Utah during Late Jurassic time, prior to initiation of thrusting in the Sevier belt and foreland basin formation. We suspect that many such topographic warps are due to variations in intraplate stress fields generated by, sometimes small, changes in global plate geometry. That these warps are associated with older structures implies simply that these structures represent long-lived zones of weakness within the continental lithosphere.

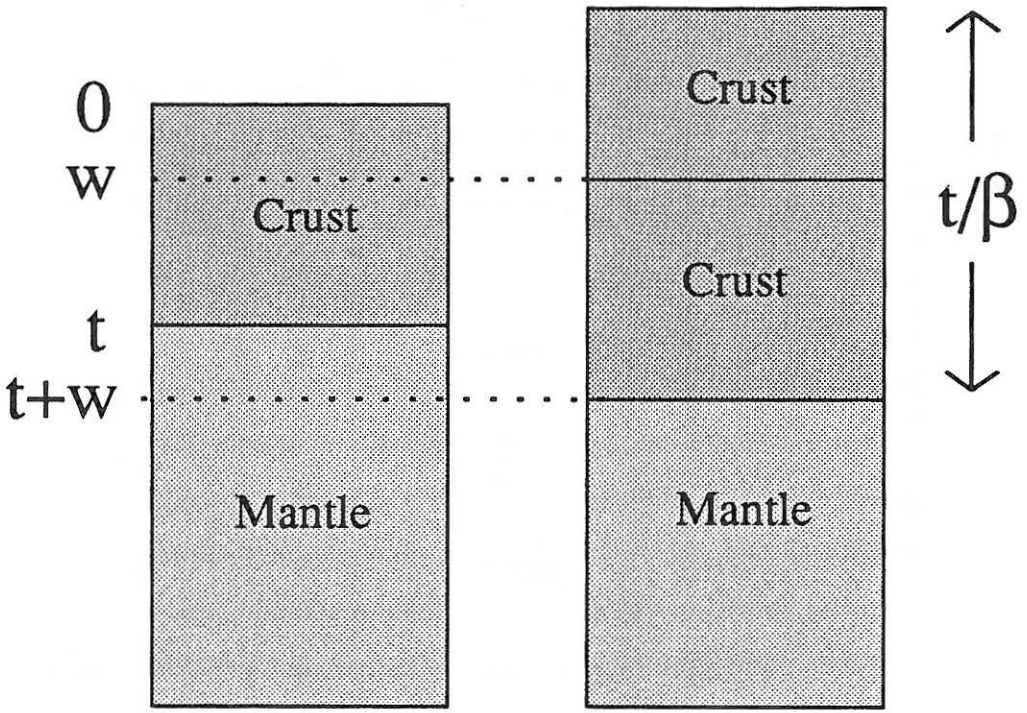

Figure 5.1 Local isostatic balance between normal (left) and thickened crust (right). The crust subsides an amount *w* into the mantle due to the weight of the added crust.

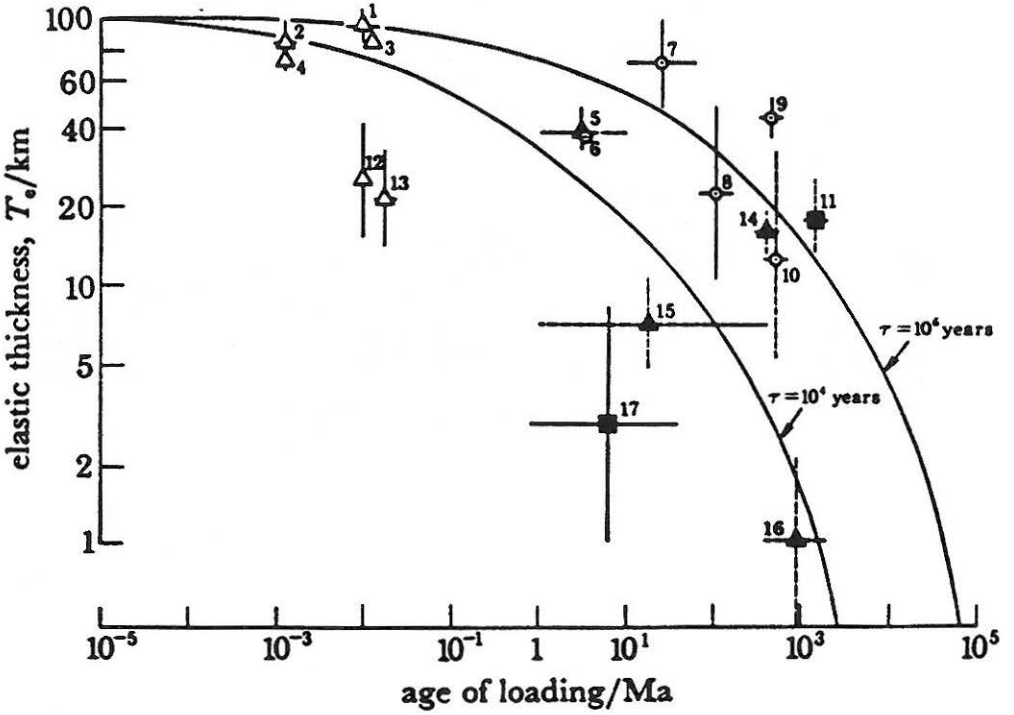

Figure 5.2 Variation in effective elastic thickness (*EET*) of continental lithosphere as a function of the age of loading (from Watts et al., 1982). The assumption that the lithosphere responds to loading like an elastic plate is justified by the observation that the lithosphere maintains its rigidity when loaded.

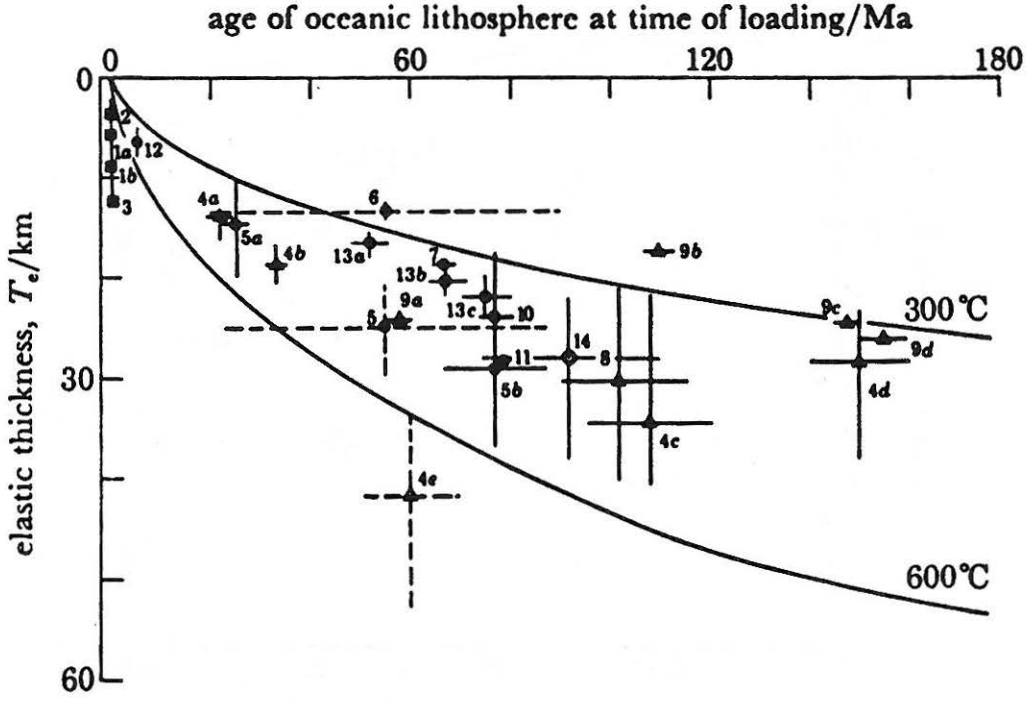

Figure 5.3 Effective elastic thickness of the oceanic lithosphere as a function of the age of the lithosphere at the time of load emplacement (also from Watts et al., 1982). Old cold lithosphere is more rigid than young hot lithosphere.

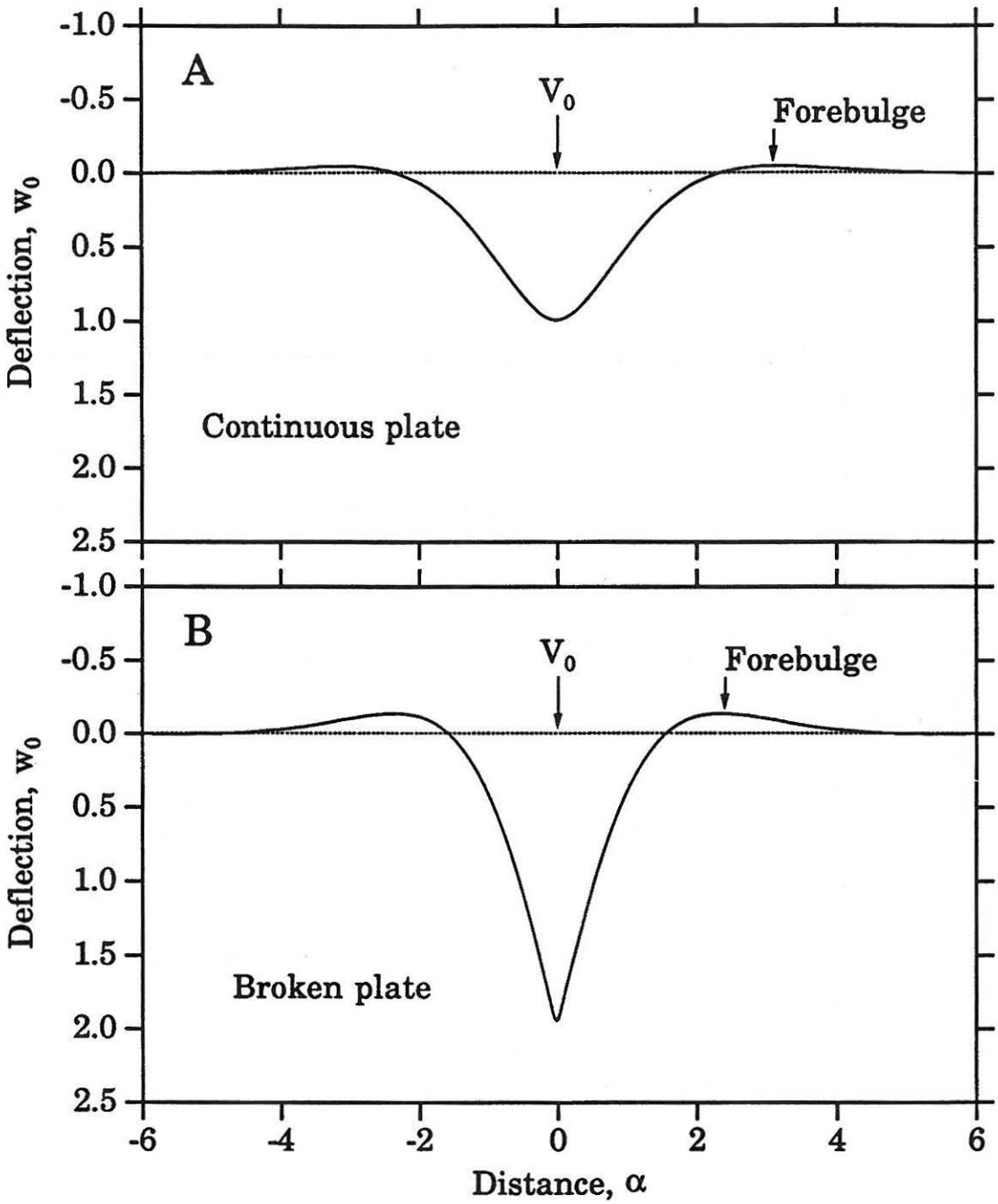

Figure 5.4 (A) Deflection of a continuous (infinite) elastic plate under a line load of strength V_0. (B) Deflection of a broken (semi-infinite) elastic plate under a line load of strength V_0. The horizontal axis is scaled by the flexural parameter α, the vertical axis by the maximum deflection w_0 of the continuous plate.

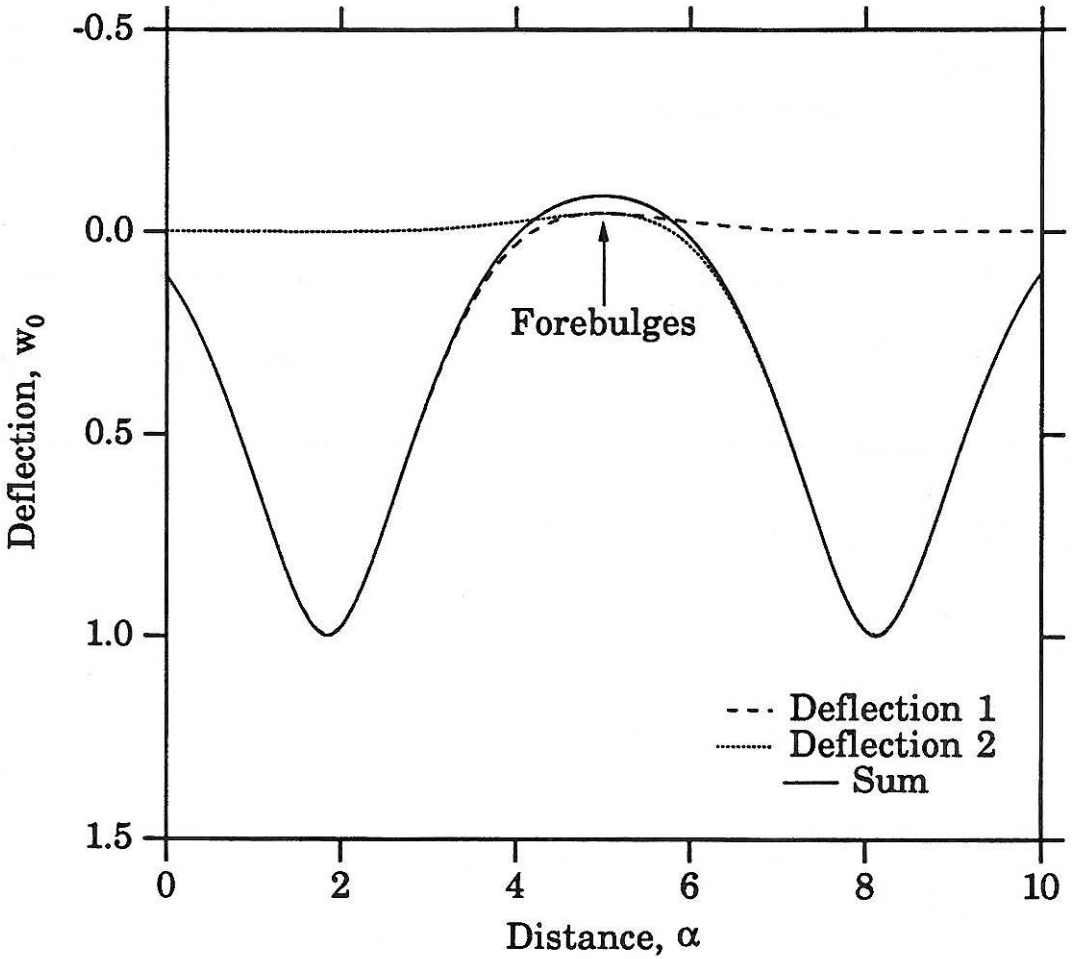

Figure 5.5 Constructive interference of forebulges associated with two parallel line loads separated by a distance of $2\pi\alpha$. The elastic flexure equation is linear, so the total deflection is equal to the sum of the individual deflections.

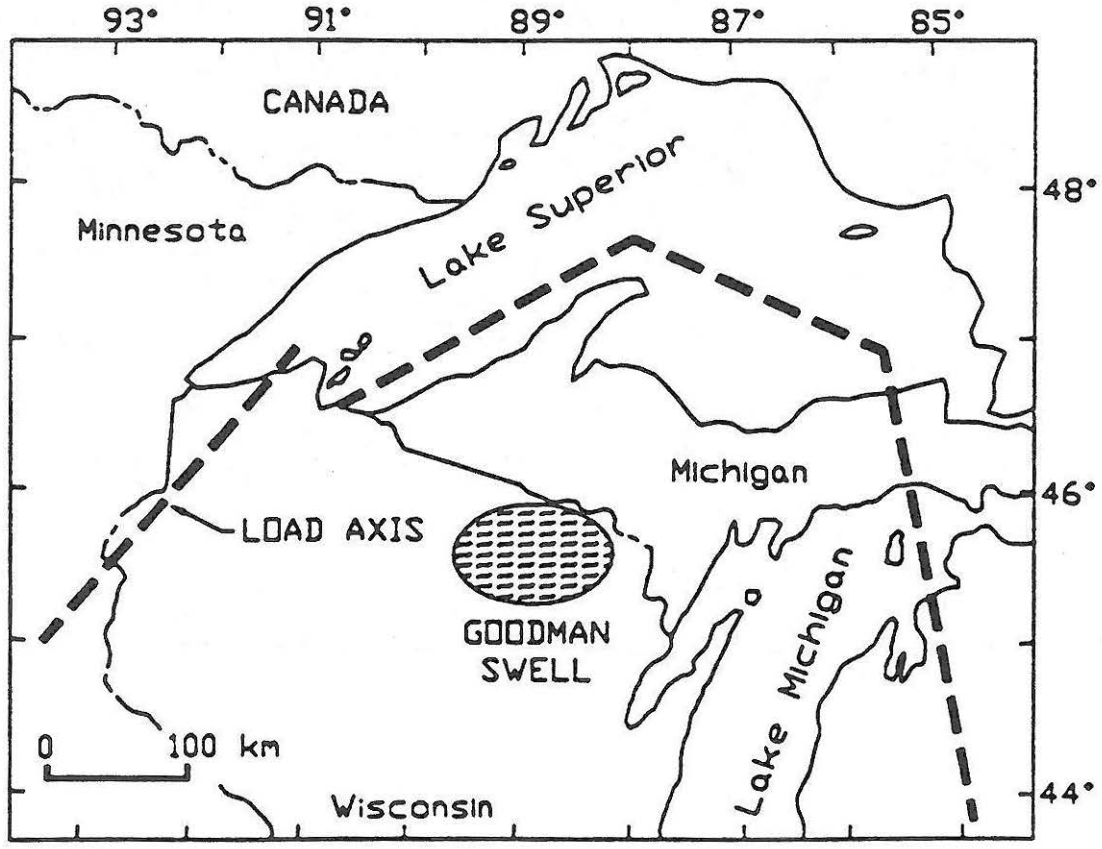

Figure 5.6 From Peterman and Sims (1988). Dashed line shows the inferred axis of maximum load along the Midcontinent rift system. Crustal ages (Rb-Sr biotite ages) on the Goodman swell are approximately 700 my younger than in surrounding areas. Goodman swell is interpreted to be a forebulge amplified by constructive interference.

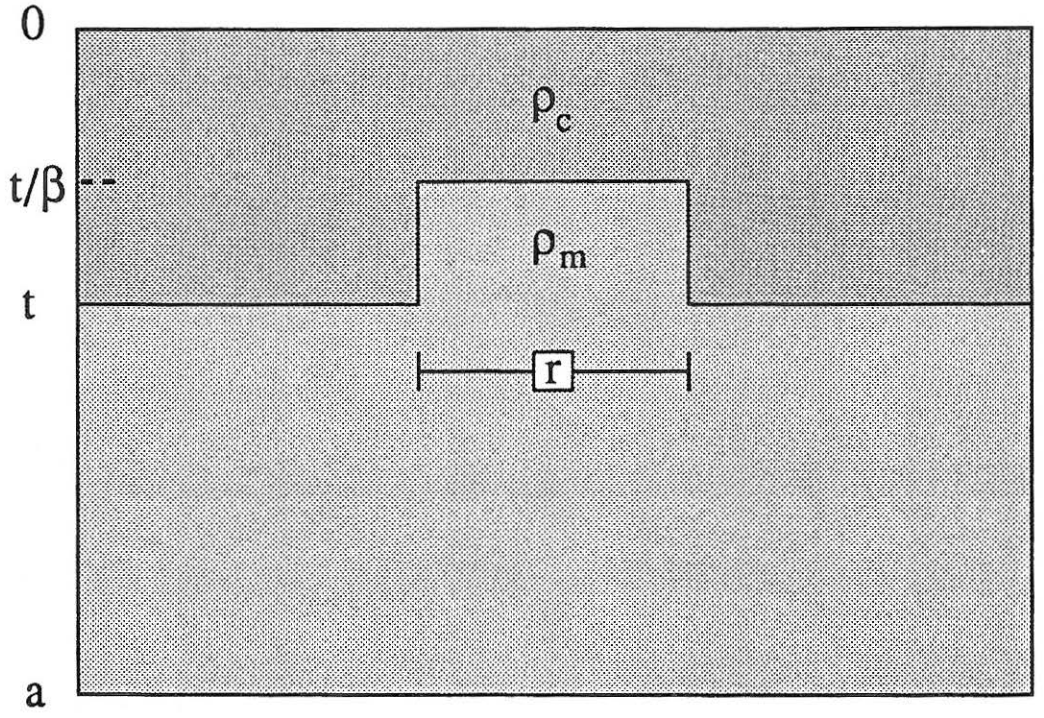

Figure 5.7 Schematic drawing of section of rifted lithosphere for the aulocogen problem. Replacement of lower crust by mantle creates an isostatic imbalance that must be compensated by lithospheric flexure.

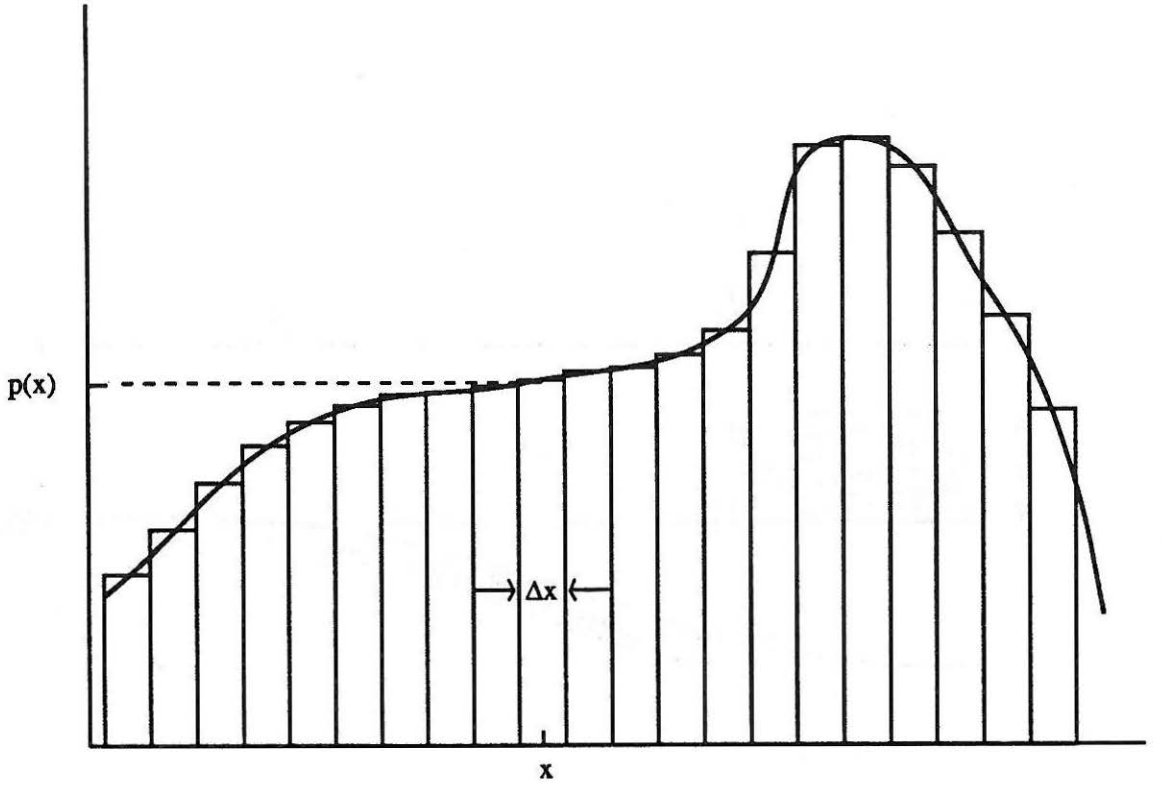

Figure 5.8 Diagram showing how a complicated load distribution can be broken into a series of line loads. Each line load has a magnitude $p(x)\Delta x$ that depends on its position.

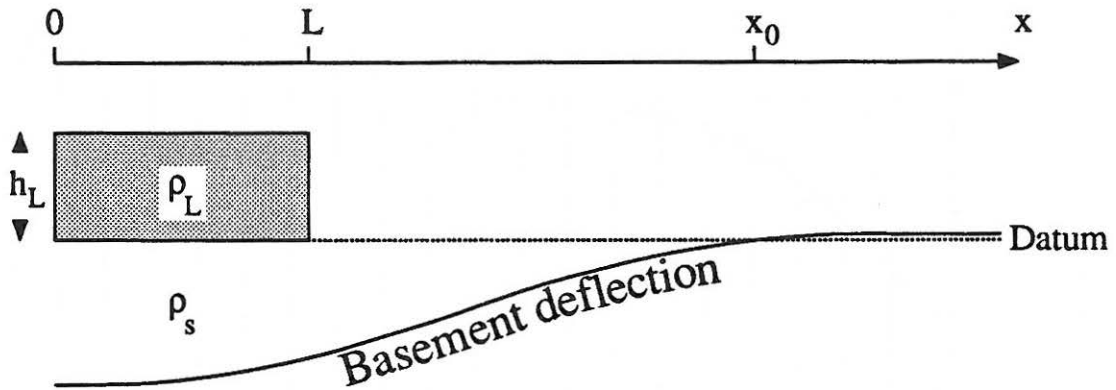

Figure 5.9 Diagram showing the deflection of the elastic lithosphere due to a load of rectangular cross section. The load has a half-width of L, an amplitude of h_L, and a density of ρ_L. Density of material filling the deflection is ρ_s. The deflection's half-width is x_0. Both load and deflection are symmetric around $x = 0$.

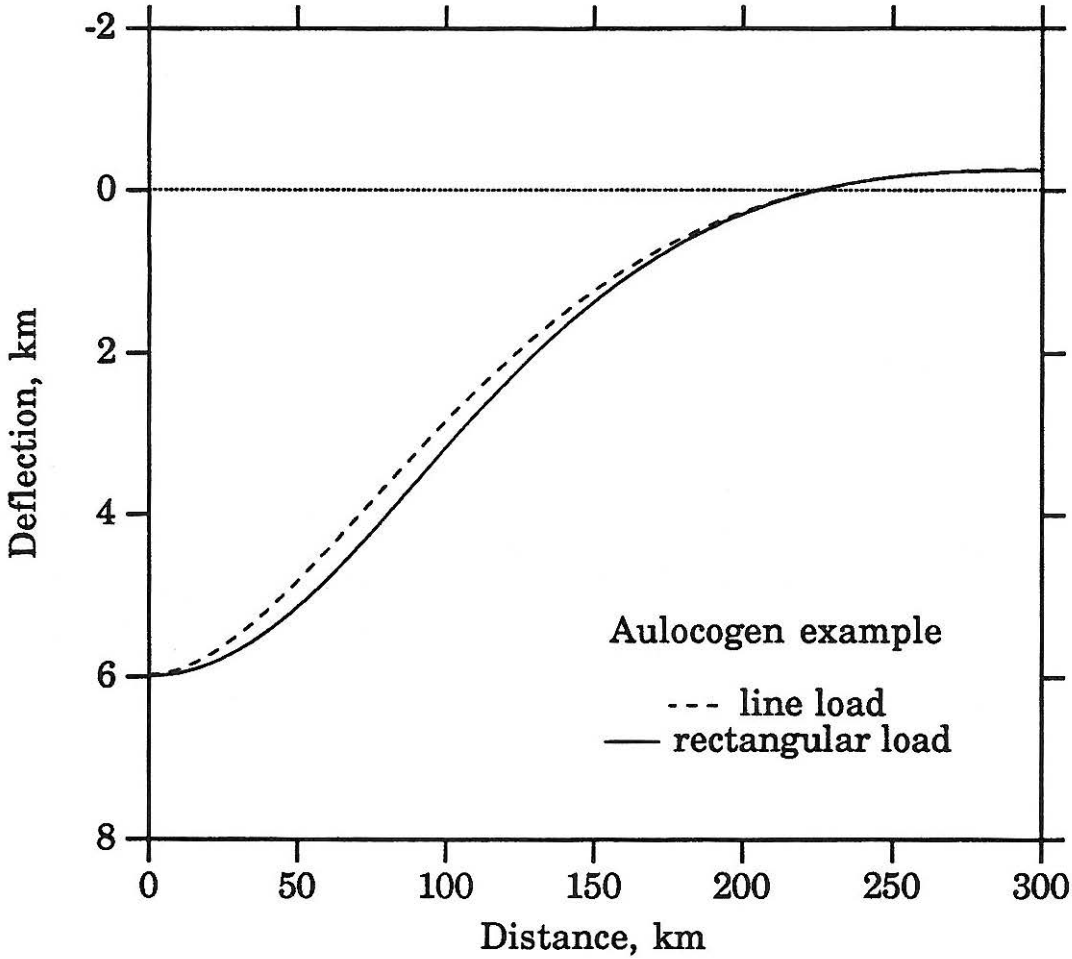

Figure 5.10 Deflection of lithosphere under a line load and distributed rectangular load. Parameters come from Examples I and II, the aulocogen models.

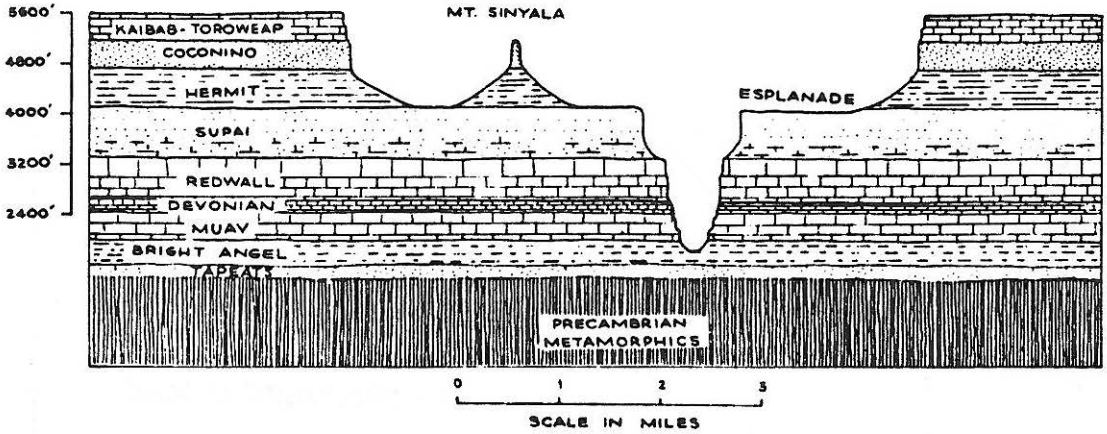

Figure 5.11 Cross-section through the Grand Canyon of the Colorado River, near Havasu Creek (from Hamblin and Rigby, 1969). See Example III.

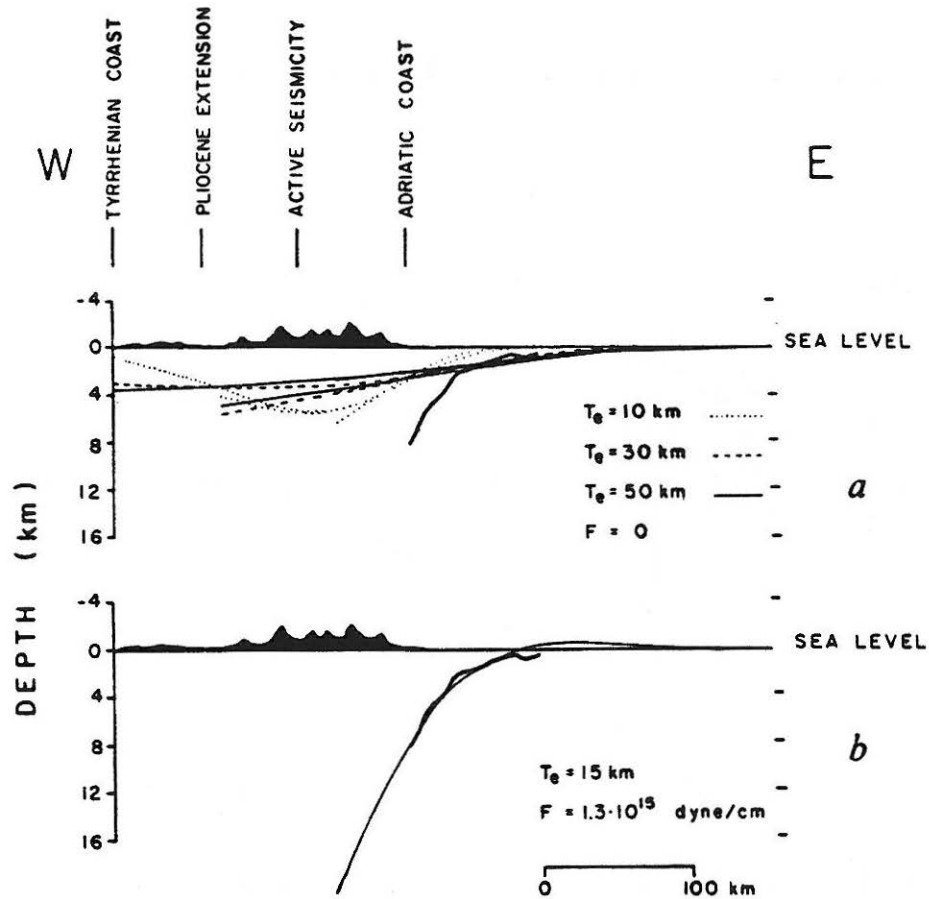

Figure 5.12 Deflection of a basal Pliocene horizon (heavy curve) in the Apennine foredeep basin (from Royden and Karner, 1984). (A) The topographic load of the thrust belt is too small to explain the observed deflection. (B) A line load is applied at the end of the broken plate (under the Apennines) to bring the theoretical and observed deflections into agreement.

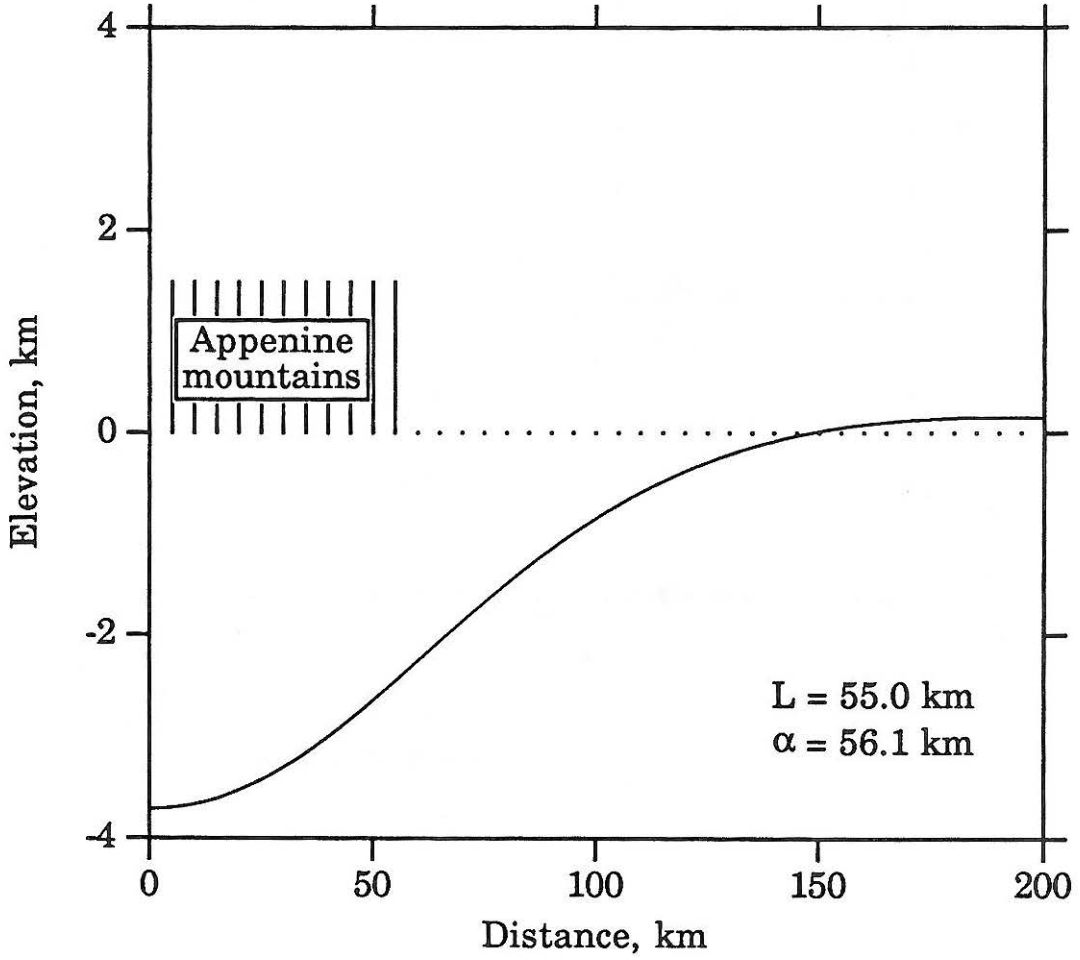

Figure 5.13 Deflection of lithosphere under a rectangular load with a halfwidth of 55 km, an amplitude of 1.5 km, and a density of 2500 kg/m^3. The rectangular load represents the topographic load of the Apennine mountains. For a flexural parameter of 56.1 km, a maximum deflection of less than 4 km is achieved under the axis of the mountains. The deflection is filled with sediment of density 2500 kg/m^3.

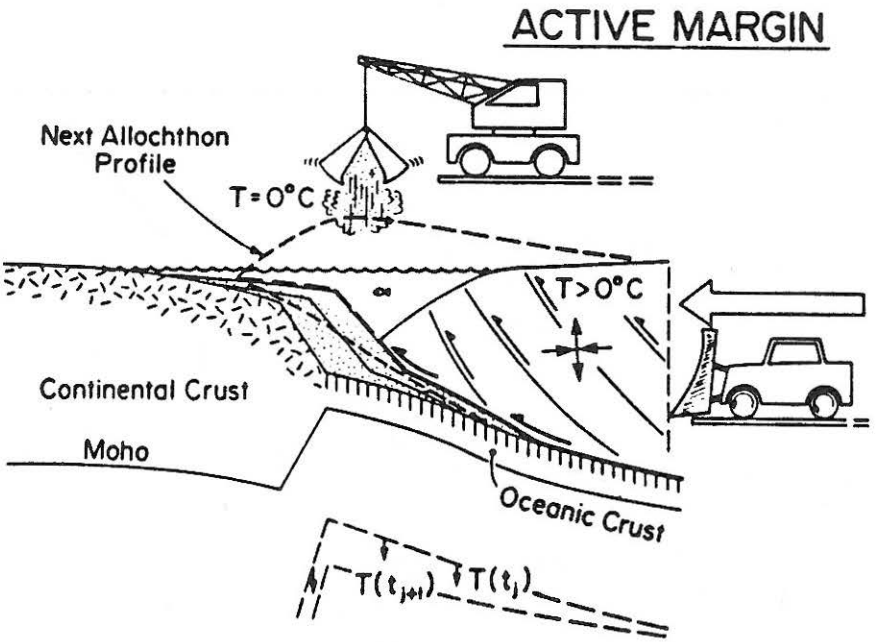

Figure 5.14 Loading of a passive margin by an advancing orogenic wedge (from Stockmal et al. 1986). The thrust belt is not built on an initially horizontal surface as was assumed in the previous figure; an ocean basin has to be filled before topography is constructed.

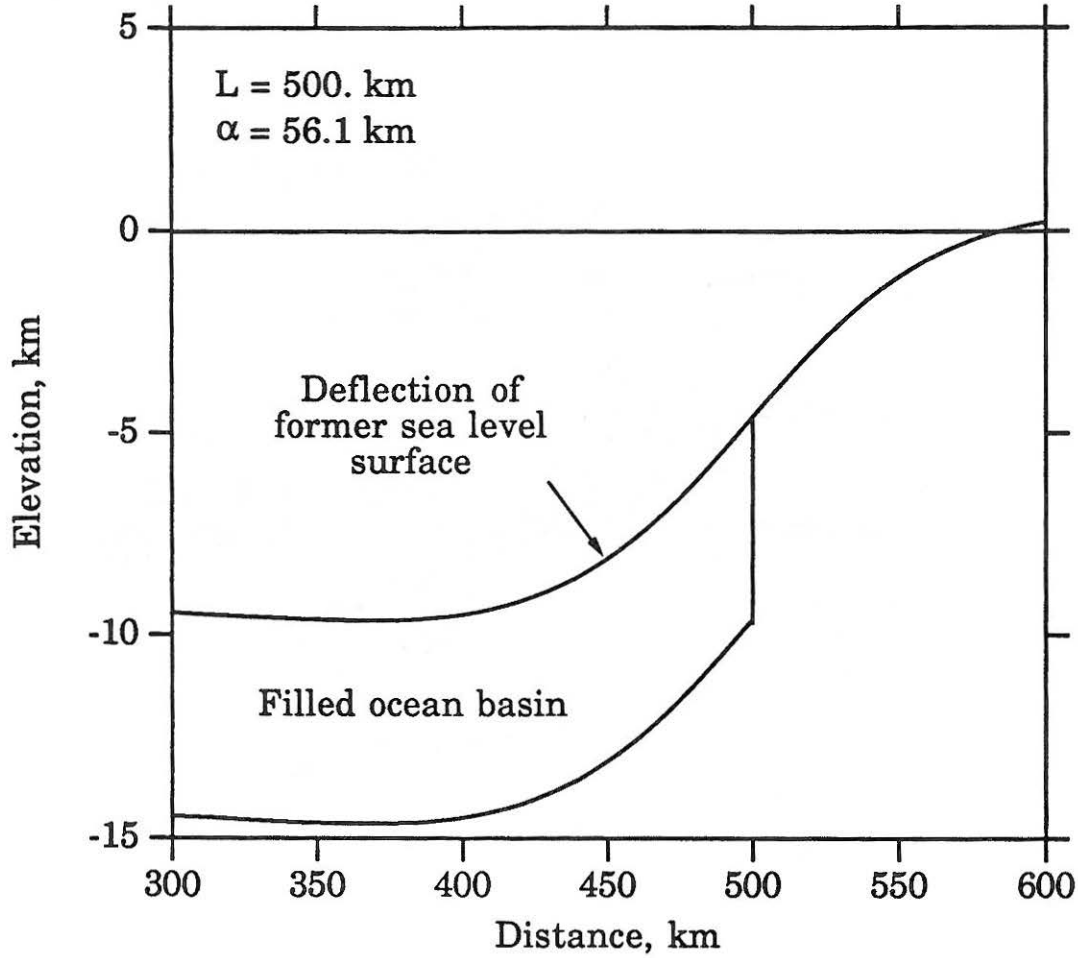

Figure 5.15 Deflection caused by replacing water in a 5-km-deep ocean basin with sediment of density 2500 kg/m^3. The deflection is also filled with sediment. The continental margin is deflected by 4.7 km.

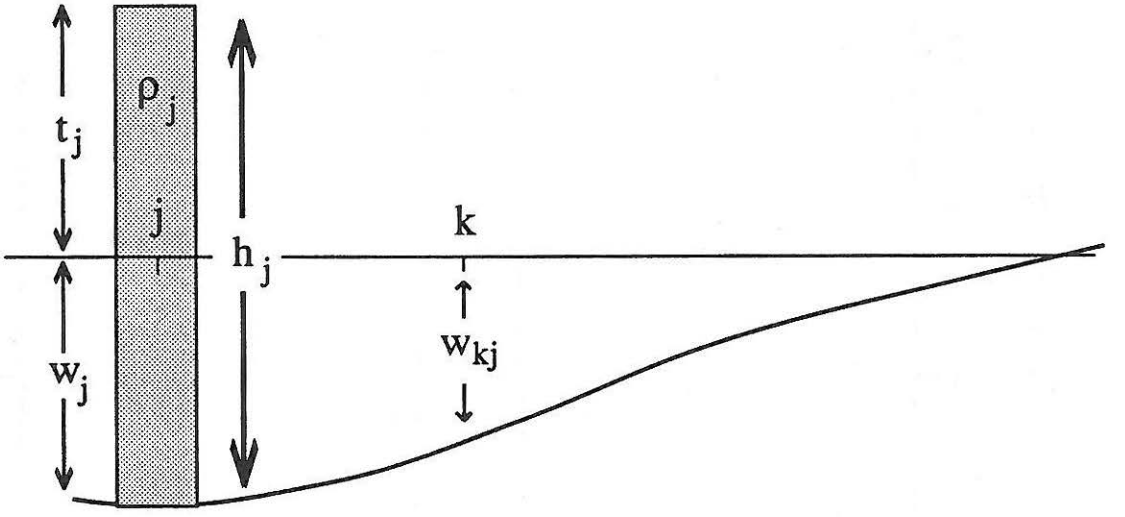

Figure 5.16 Representation of loads and deflections in deflection algorithm. At the jth point, the total deflection is w_j, the load thickness is h_j, the load topography is t_j, and the load density is ρ_j. The load at the jth point causes an incremental deflection of w_{kj} at the kth point.

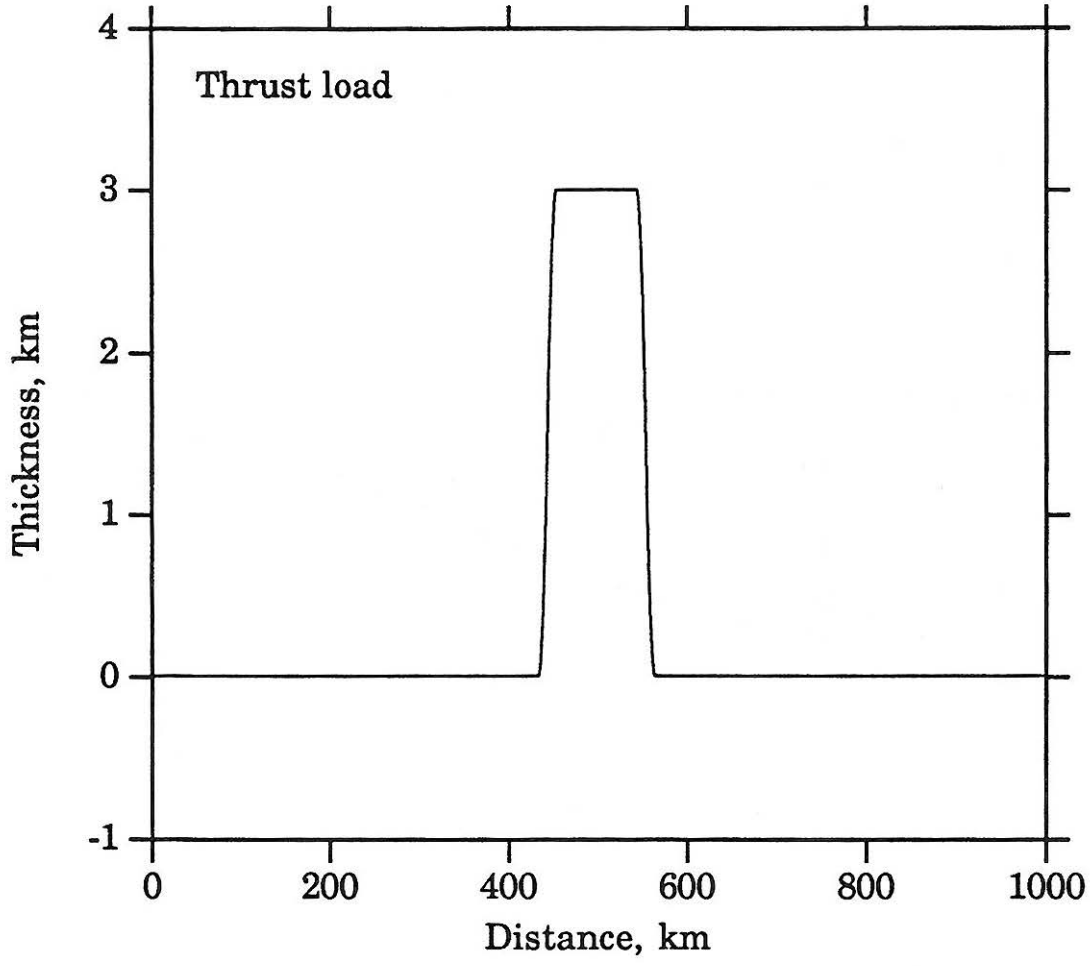

Figure 5.17 Representation of thrust belt for deflection calculation. Thrust belt is 110-km-wide by 3-km-thick with a density of 2500 kg/m^3.

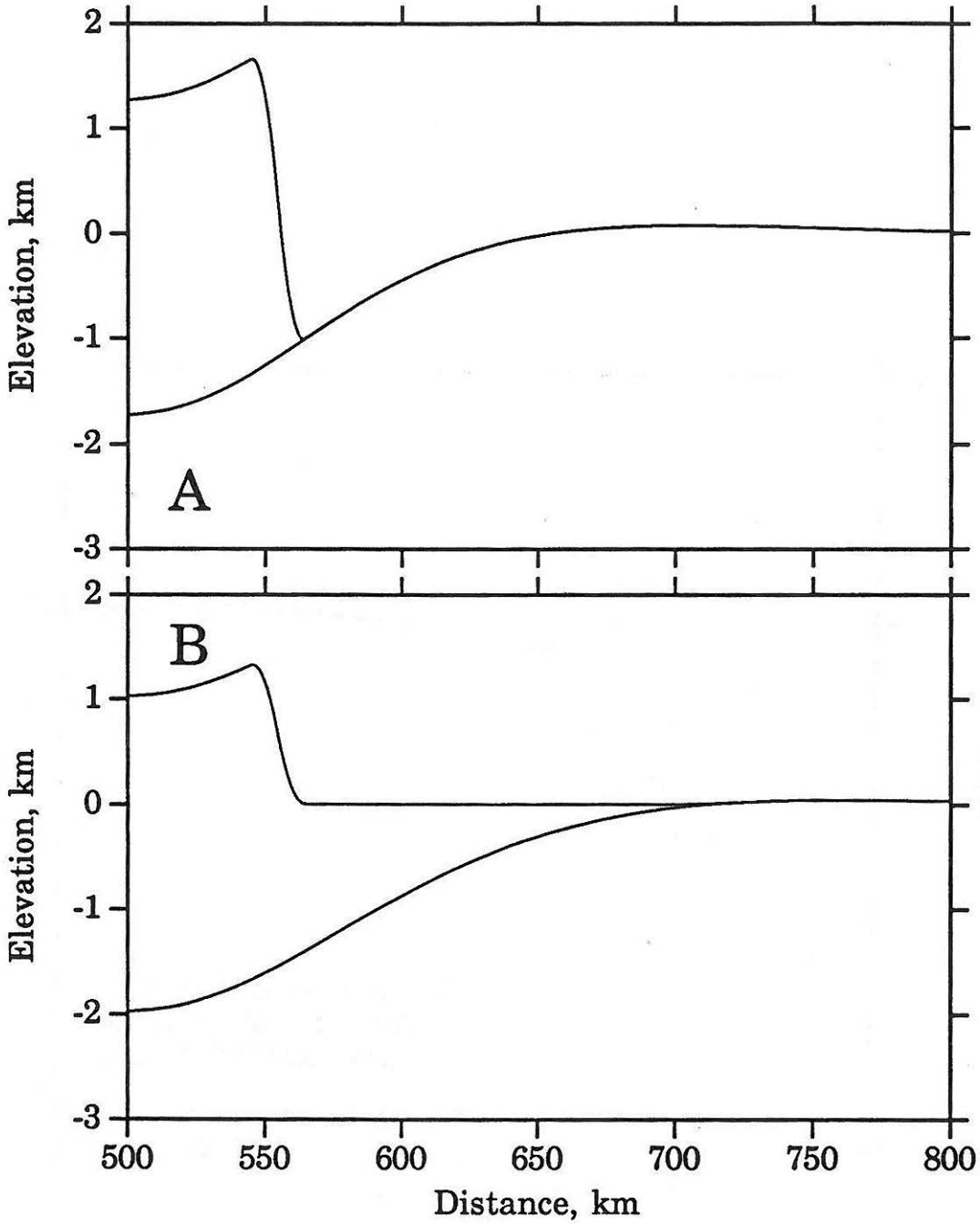

Figure 5.18 Deflection of lithosphere under load of thrust belt. The thrust belt is not entirely a topographic load; the thrust belt is allowed to sink into the deflection. (A) Deflection with no sediment (only air) loading the foredeeps. (B) Deflection with foredeep filled by sediment (ρ_s = 2300 kg/m^3).

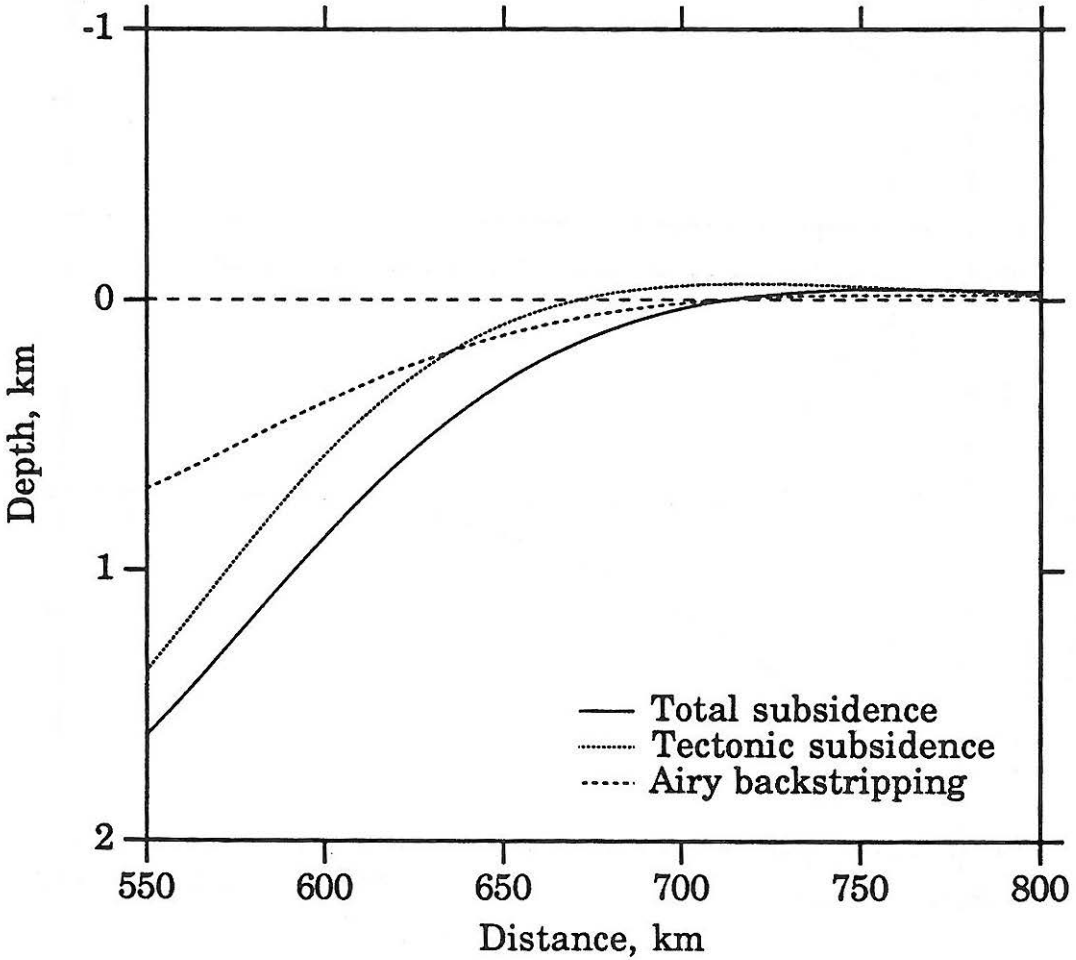

Figure 5.19 Curves showing total subsidence and tectonic subsidence in the foreland basins, from Figure 5.18. Tectonic subsidence curves are calculated assuming both regional (flexural) and Airy compensation.

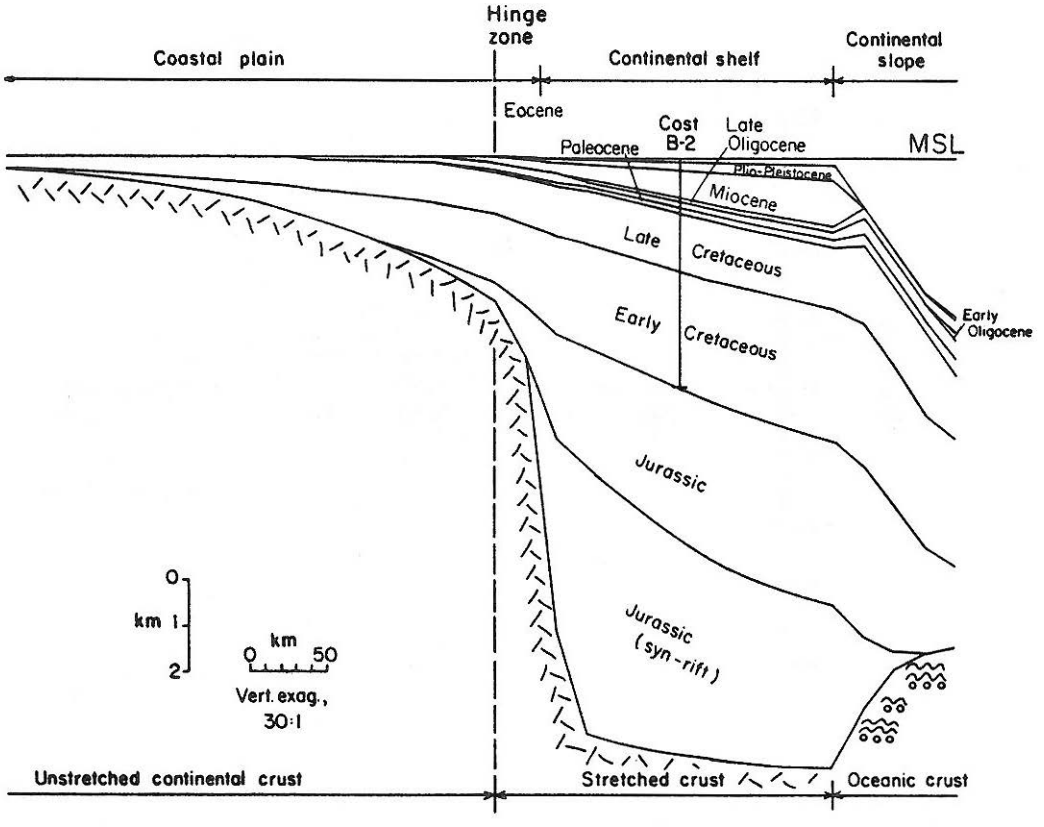

Figure 5.20 Stratigraphic section across east coast of the United States based on well and seismic reflection data (from Watts and Thorne, 1984). Middle and Late Mesozoic sediments onlap progressively onto the continent. Some of the onlap may be due to the cooling and stiffening of the lithosphere.

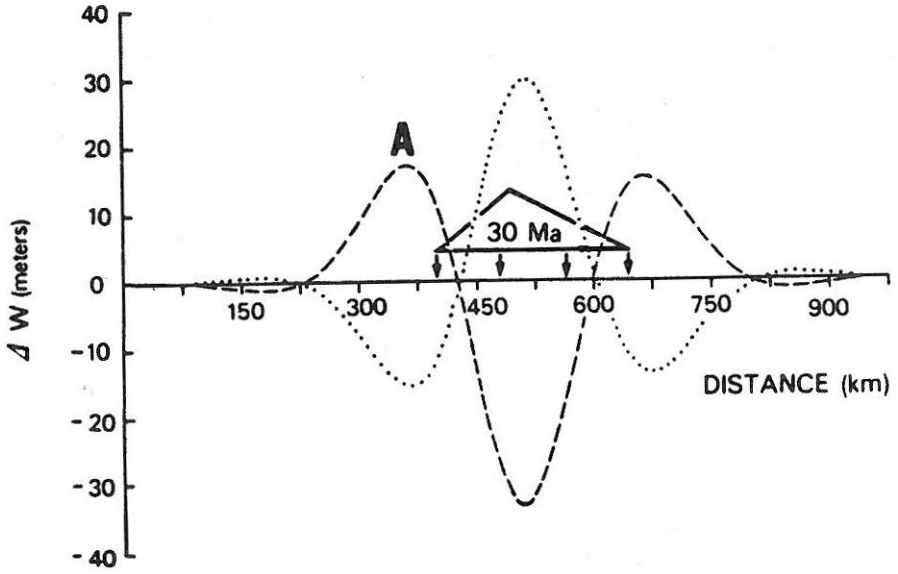

Figure 5.21 Effect of variations in the intraplate stress field on passive margin stratigraphy (from Cloetingh et al., 1985). The margin was initially locally compensated. Compressive (tensional) stress causes subsidence (uplift) in the center of the sedimentary basin and uplift (subsidence) on the margins. Stress variations may responsible for some regional sea-level fluctuations.